

# Multichannel long-range Rydberg molecules

Matthew T. Eiles and Chris H. Greene

(Dated: July 15, 2015)

A generalized class of ultra-long-range Rydberg molecules is proposed which consist of a multichannel Rydberg atom whose outermost electron creates a chemical bond with a distant ground state atom. Such multichannel Rydberg molecules exhibit favorable properties for laser excitation, because states exist where the quantum defect varies strongly with the principal quantum number. The resulting occurrence of near degeneracies with states of high orbital angular momentum promotes the admixture of low  $l$  into the high  $l$  deeply bound ‘trilobite’ molecule states, thereby circumventing the usual difficulty posed by electric dipole selection rules. Such states also can exhibit multi-scale binding possibilities that could present novel options for quantum manipulation.

Ultra-long-range Rydberg molecules were predicted some time ago for the simplest atoms in the periodic table, consisting of one ground state atom and one Rydberg atom having just one valence electron outside of a closed-shell core [1–5]. These unusual long-range Rydberg molecules have since been observed experimentally, in a number of experiments that have focused primarily on penetrating Rydberg states of low orbital angular momentum. Very recently, experimental evidence [6] of a true long-range trilobite molecule has been found, consisting of an  $ns$  Rydberg state of Cs with a large admixture of high angular momentum states that hybridize to form an electronic wavefunction with a huge kilodebye electric dipole moment.

The simplest type of such excited-ground state molecules have thus been confirmed, and the theoretical description has been generalized to include hyperfine interactions and the coupling of electronic singlet and triplet states [7]. Moreover, other interesting generalizations have been developed, such as the binding of multiple ground state atoms [8, 9], the behavior of long-range Rydberg molecules subjected to an external electric field [10–12], and even the behavior of a single Rydberg alkali atom excited in a Bose-Einstein condensate [13].

While an alkali atom Rydberg gas provides a simple and easily-controlled system for the excitation of novel molecular states, in fact Rydberg atoms throughout the rest of the periodic table are far richer and more complex, as they consist primarily of perturbed, multichannel Rydberg spectra [14–17]. The present Letter demonstrates some of the opportunities provided by this richer class of multichannel Rydberg atoms that can bind one or more ground state atoms. One finding in particular is that the existence of doubly-excited perturbors can be used in the alkaline earth atoms to directly excite long-range trilobite molecules with their exceptionally large electric dipole moments. Another possibility raised by the existence of doubly-excited perturbors is that energy eigenfunctions exist whose multichannel character exhibits two very different length scales. Such stationary states can in principle be used to trap ground state atoms at very different internuclear distances, providing opportunities for unusual types of quantum control and manipulation.

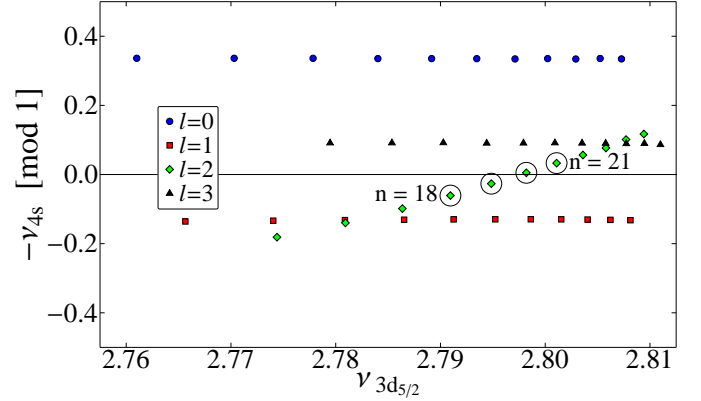


FIG. 1. A Lu-Fano plot [19] highlighting the effects of level perturbors on the quantum defects of the  $nd$  states of Ca [20], in contrast to the energy-independent behavior of the quantum defects for  $s$ ,  $p$ , and  $f$  states. The quantum number  $n$  rises from 15 to 24 from left to right. This letter investigates the circled states.

This letter focuses on the  $4snd \ ^1D_2$  levels in calcium, where perturbations from the doubly excited states  $3d4d$  and  $3d5s \ ^1D_2$  cause the  $4snd$  singlet quantum defect to vary rapidly in the vicinity of these perturbing levels [18]. Fig. 1 depicts the strong  $n$ -dependence of the  $l = 2$  quantum defects. Calcium is chosen because the d-wave quantum defects pass through unity as the principal quantum number  $n$  increases between  $n \sim 20 \pm 2$ ; the  $nd$  state is therefore highly degenerate with high angular momentum states in the  $n - 1$  manifold. This accidental degeneracy strongly couples these states together, allowing for direct two-photon excitation of trilobite molecules, circumventing the usual challenges of exciting high angular momentum states which typically require electric fields to break dipole selection rules or else an additional microwave photon after a two-photon process [1]. This removes the experimental obstacles in creating and studying these exotic long-range molecules. The interaction between the nearly-free Rydberg electron and the ground state perturber can be simply and accurately described

by the Fermi pseudo-potential [2]

$$V_{pp}(\vec{r}, \vec{R}) = 2\pi a_s[k(R)]\delta^3(\vec{r} - R\hat{z}) + 6\pi a_p[k(R)]\delta^3(\vec{r} - R\hat{z})\vec{\nabla} \cdot \vec{\nabla}, \quad (1)$$

where the energy-dependent s-wave scattering length and p-wave scattering volume are respectively,  $a_s[k(R)] = -\tan \delta_0/k(R)$  and  $a_p[k(R)] = -\tan \delta_1/[k(R)]^3$ , implicitly depend on the internuclear separation  $R$  through the semiclassical kinetic energy  $\frac{1}{2}k(R)^2 = E_{nl} + \frac{1}{R}$ . The internuclear axis points in the  $\hat{z}$  direction. The energy-dependent phase shift data used to calculate these scattering properties were calculated by [22]. Both earlier [5] and recent [24] work has emphasized that diagonalization using this delta-function pseudopotential is formally non-convergent, but comparison with more complicated Green function or Kirchhoff integral methods [11, 23] shows that nevertheless the models agree to first order. Quantitative accuracy with experimental data within the pseudopotential model can be achieved by fitting the scattering lengths to observed spectra [25].

Two characteristics of the phase shifts differentiate this interaction in calcium from those previously studied in the alkalis. Since calcium does not possess the p-wave shape resonance that significantly modifies the potential curves of the alkali dimers [22, 26], the potential wells at all but very small internuclear distances are determined almost entirely by s-wave electron-atom scattering properties. The second contrast is that the p-wave phase shift is negative except at very low energies, so the scattering volume is positive over nearly the entire range of internuclear distances. These two differences eliminate the strongly attractive p-wave interactions present in the alkalis that support “butterfly” type bound states [27], and instead the p-wave interaction produces a weakly repulsive potential. Bound states could possibly form in this repulsive potential in the presence of a second perturber [21].  $\text{Ca}^-$  also exists as a bound negative ion with binding of the doublet  $P$  electron by  $24.55 \pm 10$  meV for  $J = 1/2$  and by  $19.73 \pm 10$  meV for  $J = 3/2$ , whereas in triplet e-Rb and e-Cs there is no stable negative ion. [29]

Adiabatic potential energy curves for  $18 \leq n \leq 21$  calculated by basis set diagonalization are presented in Fig. (2a). As  $n$  increases the  $(n+1)d$  state sweeps downwards through the  $n$  manifold, and for  $n = 19, 20$  in particular it is strongly mixed into the trilobite state. This systematic change of quantum defects with energy, caused by familiar level perturbations in multichannel spectroscopy [14], is ubiquitous in the heavier alkaline earth metal atoms and in most other atoms in the periodic table. [1] predicts two classes of long-range Rb molecules: low-angular momentum states (a) that have been observed experimentally to admix a fractional amount of trilobite character giving them non-negligible permanent electric dipole moments [30], and (b) the trilobite molecules themselves, consisting of an admixture of high angular momentum

states. The states shown here in Ca have a level of mixing intermediate between these two regimes, akin to the recent results in Cs [6]. Typical trilobite electronic probability amplitudes in cylindrical coordinates displayed in Fig. (2b,c) demonstrate this mixing as they show a “trilobite” wavefunction superimposed over an  $f$  or  $d$ -state wavefunction.

The molecular vibrational levels seen in the potential well inset are approximately spaced at 1 GHz. Many vibrational bound states are supported in these wells, which range from 30 to 60 GHz deep. These molecules should therefore be somewhat more tightly bound than those predicted for rubidium [1, 23]. The permanent electron dipole moments associated with these molecules are in the kdebye range, allowing for the possibility of delicate manipulation of these molecules with electric and magnetic fields [31, 32].

A second example of the rich physics provided by two-electron systems is predicted by exploiting the complex channel interactions due to the fine-structure splitting to create long-range molecules that display two distinct length scales. In silicon the  $3p\ ^2P_{1/2}^o$  and  $3p\ ^2P_{3/2}^o$  ionization thresholds are separated by  $\Delta E = 287.84\text{ cm}^{-1}$ . Nonperturbative interactions between Rydberg series in different channels converging to these two thresholds require the framework of multichannel quantum defect theory (MQDT) to describe the bound states of the atom. Silicon has been studied in this framework both from a semi-empirical standpoint [34] and through nearly ab initio R-matrix calculations [14, 35, 36]. Only the salient details of the semi-empirical approach will be described here, since the references contain thorough descriptions [14, 38–40]. The elements of a diagonal short-range reaction matrix in  $LS$  coupling,  $K_{ii'}^{(LS)} = \delta_{ii'} \tan \pi \mu_i$  are treated as fit parameters by matching experimental bound states with MQDT predictions. The advantage of the  $K$ -matrix formulation is that these elements have slow energy dependence in the short-range region near the core since asymptotic boundary conditions have not yet been enforced. The  $i'$ -th linearly independent wavefunction outside of this region is

$$\Psi_{i'} = \mathcal{A} \sum_i \Phi_i(\Omega) \left[ f_i(r) \delta_{ii'} - g_i(r) K_{ii'}^{(LS)} \right], \quad (2)$$

where  $i$  labels different channels,  $\Phi_i(\Omega)$  contains the wavefunction of the atomic core and all spin and orbital angular momentum degrees of freedom of the Rydberg electron, and  $(f, g)$  are the regular/irregular solutions to the Schrödinger equation with a Coulomb potential outside of the atomic core [40]. An antisymmetrization operator is denoted here as  $\mathcal{A}$ .  $LS$  coupling, which couples the orbital and spin angular momenta separately and is described by the ket  $|(l_e l_e) L(\frac{1}{2} \frac{1}{2}) S] J M_J\rangle$  is accurate for low-lying states where the electron is near the core and exchange effects dominate [40]. This coupling

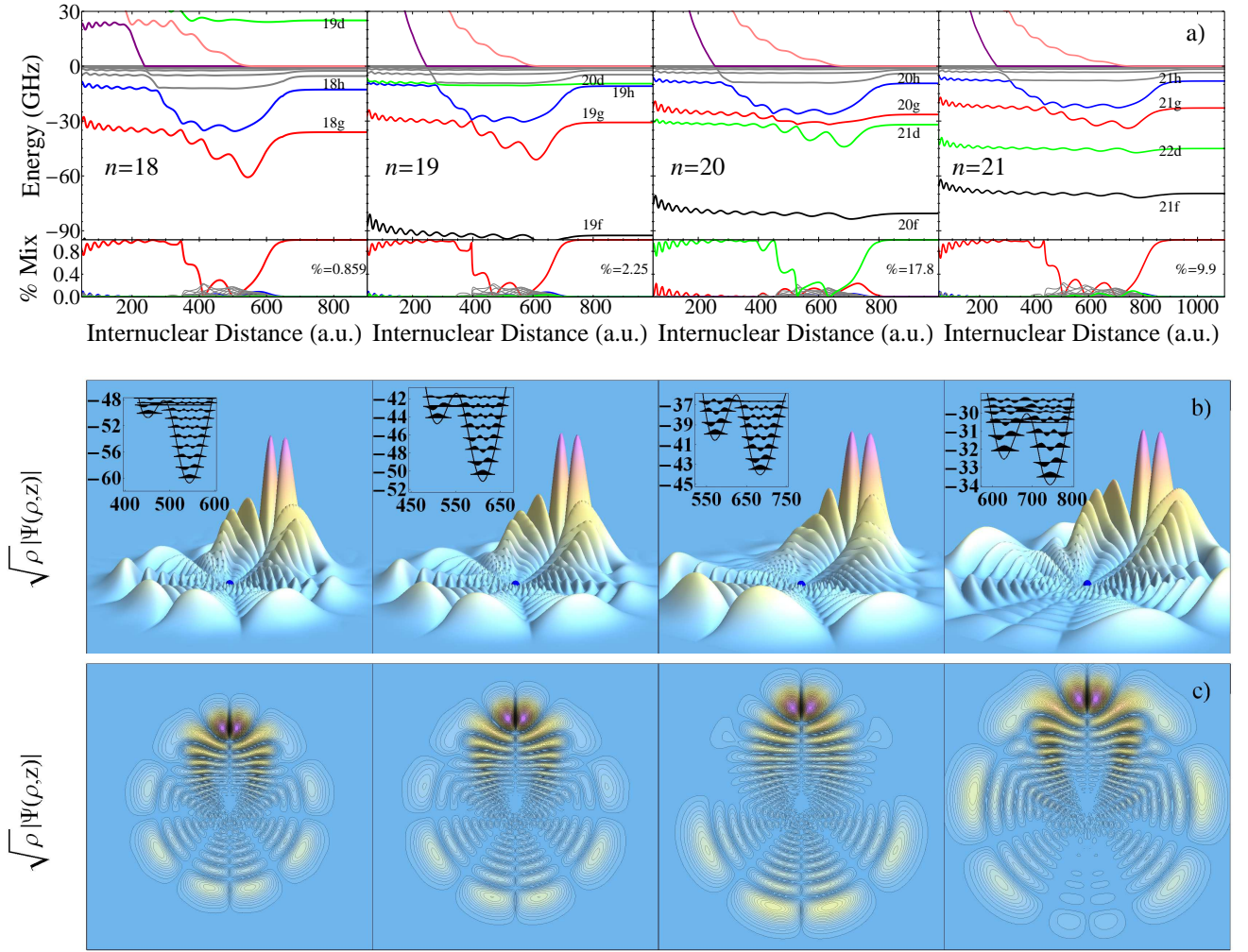


FIG. 2. a) Potential curves for  $\Omega = 0$  states, with  $n$  increasing from 18-21 from left to right. The energy scale is relative to  $-\frac{1}{2n^2}$ . The  $(n+1)d$  state descends through the degenerate manifold with increasing  $n$ . The expansion coefficients are plotted with the same color scheme, showing the locations of the trilobite states (large mixing of high angular momentum states) and importantly the amount of  $(n+1)d$  mixing in the trilobite state. The percentage labeled gives the percent contribution of the  $d$  state in the trilobites plotted in panels b) and c).

b) Electron probability amplitudes  $\sqrt{\rho}|\Psi(\rho, z)|$  in cylindrical coordinates over a region in the  $(\rho, z, 0)$  plane spanning  $(-1000, 1000)$ . This wavefunction is in the deepest minimum of the potential wells, shown in the inset along with the lowest vibrational states (in GHz, as a function of internuclear distance) of the Rydberg molecule. The Rydberg nucleus is marked by the blue sphere at the origin; the ground state atom is located in between the tallest peaks of the wavefunction at  $z \sim 600 \rightarrow 800 a_0$ . c) Contour plots of the probability amplitudes, showing the transition from primarily f-wave character outside of the trilobite wavefunction in  $n = 18, 19$  to d-wave character in 20. The scale is the same in all four graphs.

scheme breaks down at long-range where the electron accumulates radial phase at rates strongly dependent on the atomic core's total angular momentum [14]. Here a “geometric” orthogonal frame transformation matrix  $U_{ij}$ , given by standard angular momentum algebra, is used to transform into the more appropriate  $jj$ -coupling scheme represented by the ket  $|(l_c \frac{1}{2}) J_c (l_e \frac{1}{2}) J_e] J M_J\rangle$  [37]. The  $jj$ -coupled  $K$  matrix is  $K_{ii'}^{(jj)} = \sum_{jj'} U_{ij} K_{jj'}^{(LS)} U_{j'i'}^T$ . Imposition of boundary conditions at long-range requires that

$$\left( \delta_{ii'} \sin \beta_i + \cos \beta_i K_{ii'}^{(jj)} \right) B_{i'} = 0; \quad \beta_i = \pi(\nu_i - l_i). \quad (3)$$

Ensuring a vanishing determinant constrains the allowed values of  $\nu_i$  to take on discrete values, and the eigenvector  $B_i$  can be matched at long-range to an expansion in terms of re-normalized Whittaker functions  $W(r, \nu_i, l_i)$  that exponentially decay at long-range ([14] eq. 2.53):

$$\Psi_{i'} = \mathcal{A} \sum_i \left[ -\frac{B_i}{\cos \beta_i} \right] \Phi_i(\Omega) W_i(r, \nu_i, l_i). \quad (4)$$

The critical parameters in this expression are the mixing coefficients  $B_i / \cos(\pi \beta_i)$ , which determine the weighting of each channel eigenfunction in the energy eigenstate. These coefficients, as well as the bound state energies,

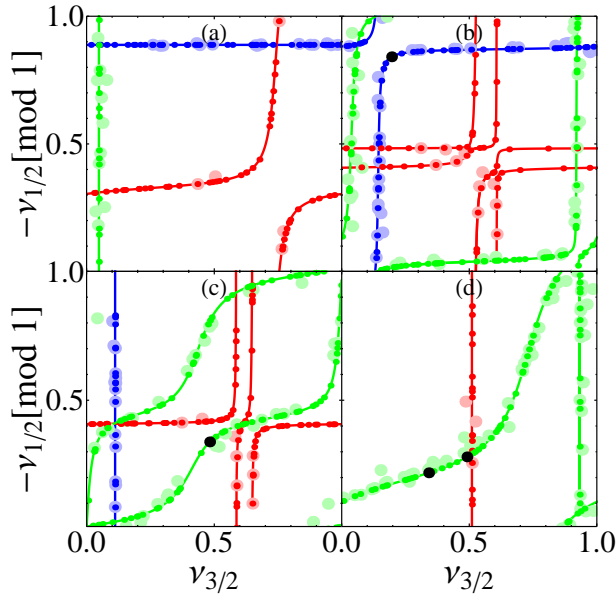


FIG. 3. Lu-Fano plots for a)  $J = 0$ , b)  $J = 1$ , c)  $J = 2$ , and d)  $J = 3$  symmetries. Blue points are  $l_e \approx 0$  odd parity; red are  $l_e \approx 1$  even parity, and green are  $l_e \approx 2$  odd parity. Larger points represent experimental levels; smaller points theoretically predicted. Black points mark the states in Fig (4)

were determined here by fitting the quantum defects  $\mu_i$  and a set of orthogonal rotation matrices to high-lying experimental levels. Spectroscopic data for  $l_e = 0, 2$  odd parity and  $l_e = 1$  even parity states with  $J = 0 - 3$  were fitted this way, with results (Fig. 3) that compare favorably with R-matrix methods [35, 36]. Most high-lying experimental energies were fitted to within  $0.5\text{cm}^{-1}$ , but the results for  $l_e = 1$  are very uncertain due to a dearth of experimental values available for fitting. The model's accuracy can be seen by comparing the larger points on Fig. 3 with the theoretical points.

The system studied here consists of a Rydberg Si atom interacting via the Fermi pseudopotential with a dilute gas of Ca ground state atoms. We focus on the low angular momentum potential curves, similar to class (a) from [1]. The p-wave contribution is non-negligible at small internuclear distances, where the potential as a result becomes repulsive. Fig. 4 displays several example potential curves. Those states exhibiting the multi-scale binding behavior predicted here lie on rapidly varying portions of the Lu-Fano plot, while primarily single-channel states fall on flat portions of these curves; hence, the  $J = 3$ ,  $l_e \approx 2$  states most consistently display deep separated wells. Panels b) and c) of Fig. (4) show two typical potential curves for this symmetry, while a) shows one of the few  $J = 1$ ,  $l_e \approx 0$  states to display two well separated deep wells, and c) shows a primarily single channel

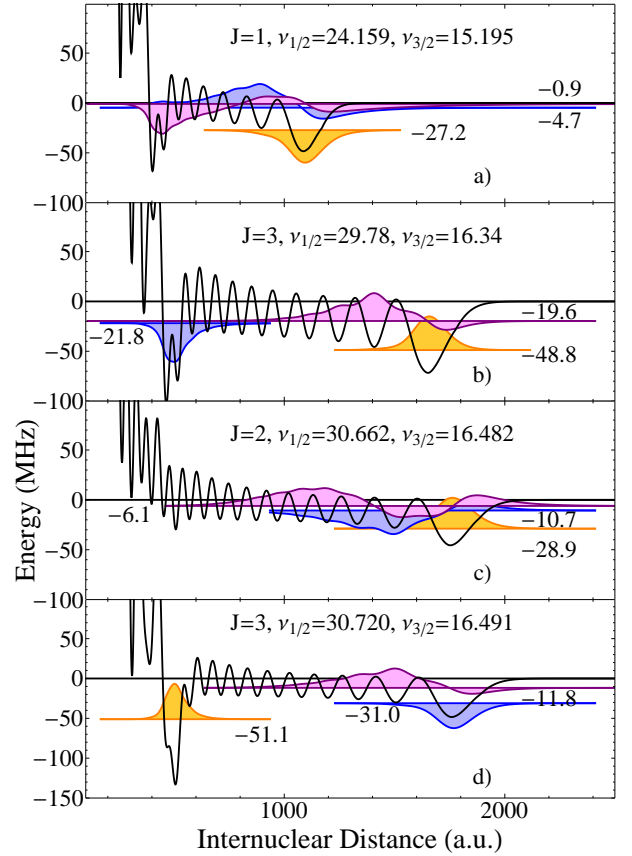


FIG. 4. Adiabatic potential curves, bound state energies, and molecular bound states for various low- $J$ , levels of the  $M_J = 0$  Si\*-Ca Rydberg molecule. The binding energies (in MHz) labeling each bound state are listed relative to the asymptotic atomic energy, which can be obtained from  $E = E_1 - 1/2\nu_{1/2}^2 = E_2 - 1/2\nu_{3/2}^2$ . We estimate an uncertainty of 0.5 MHz in these values.

case of the  $J = 2$ ,  $l_e \approx 2$  symmetry. The increasing well separation is due to the spatial scaling of each single-channel wavefunction with  $\nu_i^2$ . The potential curves are typically separated from neighboring curves by several hundred MHz or more and each support a few bound states with binding energies typically smaller than those investigated in Rb experiments [9, 25]. The ability of these potentials to support bound states is enhanced by the relatively large spin-orbit splitting and high molecular reduced mass of the Si-Ca system, but depends delicately on the energy and symmetry of the component states.

These two scenarios illustrate the rich effects of the physics of long-range multichannel molecules formed by divalent atoms. Interactions with doubly excited states in Ca allow for direct excitation of trilobite molecules through low- $l$  channels, providing a new method for experimental realization of these molecules through direct excitation. This represents a major reduction in the ex-



perimental challenges in forming these molecules, and together with recent experimental and theoretical efforts with Sr [41, 42] suggest that the alkaline atoms will be fertile fields of progress in ultralong-range molecular studies. In the Si\*-Ca molecules predicted here, the multi-channel description of the Rydberg structure predicts far richer low angular momentum potential energy curves than those studied in the alkalis, which formed bound states essentially only in the outermost well. The highly localized states in these wells should be spectroscopically accessible leading to possible applications in manipulation of the ground state atom's position across hundreds of atomic units.

We thank J. Perez-Rios and P. Giannakeas for many helpful discussions. This work is supported in part by the National Science Foundation under Grant No. PHY-1306905.

- 
- [1] C. H. Greene, A. S. Dickinson and H. R. Sadeghpour, Phys. Rev. Lett. **85**, 2458 (2000).
  - [2] E. Fermi, Nuovo Cimento **11**, 157 (1934); A. Omont, J. Phys. (Paris) **38**, 1343 (1977).
  - [3] P. Valiron, A. L. Roche, F. Masnou-Seeuws, and M. E. Dolan, J. Phys. B **17**, 2803 (1984).
  - [4] I. L. Beigman and V. S. Lebedev, Phys. Rep. **250**, 95 (1995).
  - [5] N. Y. Du and C. H. Greene, Phys. Rev. A **36**, 971 (1987). See also the erratum, *ibid.* **36**, 5467 (1987).
  - [6] D. Booth, S. T. Rittenhouse, J. Yang, H. R. Sadeghpour, & J. P. Shaffer, Science, **348**, 99 (2015).
  - [7] D. A. Anderson, S. A. Miller, and G. Raithel, Phys. Rev. A **90**, 062518 (2014).
  - [8] I. C. H. Liu and J. M. Rost, Eur. Phys. J. D **40**, 65 (2006).
  - [9] V. Bendkowsky, B. Butscher, J. Nipper, J. B. Balewski, J. P. Shaffer, R. Löw, T. Pfau, W. Li, J. Stanojevic, T. Pohl, and J. M. Rost, Phys. Rev. Lett. **105**, 163201 (2010).
  - [10] M. Kurz, and P. Schmelcher, Phys. Rev. A **88**, 022501 (2013).
  - [11] E. L. Hamilton, Ph.D. thesis, University of Colorado, (2002).
  - [12] E. de Prunelé, Phys. Rev. A **35**, 496 (1987).
  - [13] J. B. Balewski, A. T. Krupp, A. Gaj, D. Peter, H. P. Büchler, R. Löw, S. Hofferberth, and T. Pfau, Nature (London) **502**, 664 (2013).
  - [14] M. Aymar, C. H. Greene, and E. Luc-Koenig, Rev. Mod. Phys. **68**, 1015 (1996).
  - [15] U. Fano, J. Opt. Soc. Am. **65**, 979 (1975).
  - [16] M. Aymar, Phys. Rep. **110**, 163 (1984).
  - [17] T.F. Gallagher, *Rydberg Atoms* (Cambridge University Press, Cambridge, England, 2005)
  - [18] M. Aymar and M. Telmini, J. Phys. B: At. Mol. Opt. Phys. **24**, 4935 (1991).
  - [19] K. T. Lu and U. Fano, Phys. Rev. A **2**, 81 (1970).
  - [20] J. Sugar and C. Corliss, J. Phys. Chem. Ref. Data **14**, Suppl. No. 2, 1 (1985).
  - [21] I. C. H. Liu, J. Stanojevic, and J. M. Rost, Phys. Rev. Lett. **102**, 173001 (2009).
  - [22] K. Bartschat and H. R. Sadeghpour, J. Phys. B **36**, L9 (2003); J. Yuan and Z. Zhang, Phys. Rev. A **42**, 5363 (1990).
  - [23] A. A. Khuskivadze, M. I. Chibisov, and I. I. Fabrikant, Phys. Rev. A **66**, 042709 (2002); M. I. Chibisov, A. A. Khuskivadze, and I. I. Fabrikant, J. Phys. B **35**, L193 (2002).
  - [24] C. Fey, M. Kurz, P. Schmelcher, S. T. Rittenhouse, and H. R. Sadeghpour, New J. Phys. **17** 055010 (2015).
  - [25] V. Bendkowsky, B. Butscher, J. Nipper, J. B. Balewski, J. P. Shaffer, R. Löw, T. Pfau, Nature (London) **458** 1005 (2009).
  - [26] C. Bahrim, U. Thumm and I.I. Fabrikant, Phys. Rev. A **63** 042710 (2001).
  - [27] E. L. Hamilton, C. H. Greene, and H. R. Sadeghpour, J. Phys. B **35**, L199 (2002).
  - [28] N. Y. Du and C. H. Greene, J. Chem. Phys. **90**, 6347 (1989).
  - [29] T. Andersen, Phys. Rep. **394**, 157 (2004).
  - [30] W. Li, T. Pohl, J. M. Rost, S. T. Rittenhouse, H. R. Sadeghpour, J. Nipper, B. Butscher, J. B. Balewski, V. Bendkowsky, R. Löw, and T. Pfau, Science **334**, 1110 (2011).
  - [31] M. Kurz, M. Mayle, and P. Schmelcher, Europhys. Lett. **97**, 43001 (2012).
  - [32] I. Lesanovsky, P. Schmelcher, and H. R. Sadeghpour, J. Phys. B **39**, L69 (2006).
  - [33] R. González-Férez, H. R. Sadeghpour, and P. Schmelcher, New J. Phys. **17** 013021 (2015).
  - [34] C. M. Brown, S. G. Tilford, and M. L. Ginter, J. Opt. Soc. Am. **65**, 385 (1975); D. S. Ginter, M. L. Ginter, and C. M. Brown, J. Chem. Phys. **85**, 6530 (1986); D. S. Ginter and M. L. Ginter, J. Chem. Phys. **85**, 6536 (1986).
  - [35] F. Robicheaux and C. H. Greene, Phys. Rev. A **47**, 4908 (1993).
  - [36] L. Kim and C. H. Greene, Phys. Rev. A **36**, 4272 (1987); **38**, 5953 (1988).
  - [37] C. M. Lee and K. T. Lu, Phys. Rev. A **8**, 1241 (1973); C. H. Greene, J. Opt. Soc. Am. B **4**, 775 (1987).
  - [38] M. J. Seaton, Rep. Prog. Phys. **46**, 167 (1983), and references therein.
  - [39] W. E. Cooke and C. L. Cromer, Phys. Rev. A **32**, 2725 (1985).
  - [40] U. Fano and A. R. P. Rau, *Atomic Collisions and Spectra* (Academic, Orlando, 1986).
  - [41] B. J. DeSalvo, J. A. Aman, F. B. Dunning, T. C. Killian, H. R. Sadeghpour, S. Yoshida, J. Burgdörfer, arXiv:1503.07929 (2015).
  - [42] C. L. Vaillant, M. P. A. Jones, and R. M. Potvliege, J. Phys. B **47**, 155001 (2014).